IEEE Open Journal of
Ultrasonics, Ferroelectrics, and Frequency Control

Received 22 February 2023; revised 9 May 2023 and 9 June 2023; accepted 22 June 2023.
Date of publication 27 June 2023; date of current version 6 July 2023.

Digital Object Identifier 10.1109/OJUFFC.2023.3289783

Formation Anisotropic Constants From Sonic Data Acquired While Drilling

BIKASH K. SINHA [1] (Life Fellow, IEEE), AND QINGTAO SUN [2]

[1] Acoustics Research, Schlumberger-Doll Research, Cambridge, MA 02139 USA *(Retired)*
[2] Halliburton, Houston, TX 77032 USA

CORRESPONDING AUTHOR: B. K. SINHA (bikashsinha48@yahoo.com)

ABSTRACT Formation anisotropic constants play an important role in the determination of formation stresses, fractures, lithology, and mechanical properties. These formation characteristics provide critical inputs to wellbore stability during drilling and optimal completion designs of hydrocarbon bearing reservoirs. However, there are no available techniques for the estimation of a sub-set of formation anisotropic constants using Logging-While-Drilling (LWD) sonic data. Inversion of LWD-sonic data for anisotropic constants is rather challenging because of a strong coupling between the collar-flexural and formation-flexural modes propagating along the borehole. The influence of a strong coupling between the collar and formation flexural modes on LWD-sonic data are significantly different in fast and slow formations. Consequently, frequency dependent sensitivities of the measured collar and formation flexural dispersions to changes in the formation anisotropic constants are significantly different as well. New inversion algorithms provide estimates of a sub-set of Transversely-Isotropic (TI)-constants from measured collar and formation flexural dispersions in both fast and slow formations. Computational results confirm validity of the proposed algorithms using synthetic dispersion data obtained in a fast Bakken shale and slow Austin chalk TI-formations in the presence of a drill-collar to account for the LWD sonic tool in a liquid-filled borehole.

INDEX TERMS Formation anisotropic constants from Logging-While-Drilling (LWD) sonic tools, inversion of drill-collar and formation-flexural mode dispersions for formation TI-constants, geophysical and geomechanical measurements, sonic well logging.

I. INTRODUCTION

SONIC logging has a lot more potential to provide several geophysical, geomechanical, and petrophysical formation properties than is generally obtained in the oil and gas industry [1], [2], [3], [4]. Many of these formation properties are derived from formation anisotropic constants associated with formations in the presence of either stresses, drilling-induced and natural fractures, microlayerings or thin laminations [5], [6], [7], [8], [9], [10]. However, to estimate formation anisotropic parameters requires inversion algorithms that account for the presence of Logging-While-Drilling (LWD) or wireline sonic tools in the borehole and a detailed understanding of the rock lithology and facies that has been logged. Estimates of anisotropic constants using LWD sonic tool data has the potential to obviate a need to run wireline sonic tool that would reduce the cost of completing the well for hydrocarbon production. Therefore, it is desirable to have a reliable LWD tool model to account for any interactions between the tool and formation modes propagating along the borehole. In addition, model-based inversions of borehole guided mode dispersions are needed to estimate formation anisotropic constants for both fast and slow formations.

Borehole guided-mode propagation characteristics in a concentrically placed drill-collar in fast and slow formations are significantly different. For example, refracted shear headwaves are not detected by hydrophone receivers placed in the LWD sonic tool in slow formations. Therefore, estimation of formation shear slownesses is rather challenging, and is, generally, not attempted using a dipole transmitter in a LWD sonic tool. This has led to an effort to log quadrupole modes that are largely independent of the drill-collar modes and can be processed to yield formation shear slownesses at low frequencies. Nevertheless, an array of hydrophone receivers record waveforms that can be processed to identify a bandlimited collar-flexural and formation-flexural dispersive modes.

Both the collar-flexural and formation-flexural dispersions can be inverted with the help of a model- based algorithm to yield accurate estimates of formation shear slownesses and a subset of formation TI-constants.

Historically, Logging-While-Drilling (LWD) sonic tools provide estimates of formation compressional velocity from the measured transit times of compressional headwaves. Recent introduction of *dipole* and *quadrupole* transmitters in the logging-while-drilling (LWD) sonic tools enable estimates of shear velocity in both fast and slow formations. A generic LWD sonic tool consists of a thick drill collar placed in a liquid-filled borehole surrounded by anisotropic formations. The presence of a thick drill collar introduces a strong collar mode that interferes with the formation mode propagating along the borehole axis. A strong coupling between these propagating modes makes conventional processing of recorded waveforms rather challenging. A conventional processing of sonic waveforms is based on frequency-filtering or time-windowing of an array of recorded waveforms that often lead to a certain degree of uncertainty in the shear slowness estimates unless they are verified by estimates from a wireline sonic tool [11]. In addition, the dominant collar mode in the recorded waveforms in slow formations deters estimates of formation shear slownesses using conventional processing techniques. These observations have led to the introduction of a quadrupole transmitter that generates formation quadrupole mode. The formation quadrupole mode is essentially not affected by the presence of drill collar over a limited bandwidth and low-frequency part of quadrupole dispersion is rather close to the formation shear slowness [14], [15], [16]. Consequently, quadrupole shear logging was introduced in the LWD sonic tools as a way to avoid processing of dipole flexural waveforms, because of a strong coupling with the dominant collar-flexural mode [14], [15], [16], [17], [18], [19]. All existing processing techniques to estimate formation shear slownesses from LWD sonic waveforms are based on filtering out collar arrivals in fast formations and then using a conventional Slowness-Time-Coherence STC processing of an array of recorded waveforms [11]. However, none of these processing algorithms can provide estimates of a subset of formation TI-constants.

Conventional processing of dipole flexural waveforms from a LWD sonic tool is rather challenging, because of a strong coupling of the collar-based and formation-based modes. This article describes a novel processing workflow to estimate formation slownesses in both fast and slow formations. This workflow is based on inverting the measured collar-based and formation-based dispersions for formation elastic constants that can be readily transformed into formation compressional and shear slownesses. These processing algorithms account for the presence of drill collar and there is no need to suppress or filter any of these modes propagating along the borehole. Guided mode dispersion sensitivities to formation TI-constants can be calculated from an integral equation that relates fractional changes in formation TI-constants to corresponding changes in the dispersive mode velocities. A set of these equations at multiple frequencies (or wavenumbers) can then be inverted to estimate a subset of formation TI-constants.

Most of the applications of sonic data are based on an appropriate interpretation of anisotropic constants in conjunction with the logged formation lithology. For instance, relative magnitudes of shear moduli in stress-dependent sandstones and carbonates can be used to estimate differences in the maximum and minimum horizontal stresses. They can also be used to estimate orientations of aligned fractures or laminates in the formation with respect to the borehole axis [6], [7], [9], [10].

Estimates of compressional and shear velocities in anisotropic formations require a proper model-based interpretation that must account for the presence of thick drill collar in a liquid-filled borehole. The presence of a drill collar causes significant changes in elastic wave propagation characteristics that must be accounted for a reliable interpretation of compressional and shear wave velocities as well borehole guided-mode dispersions [26], [28].

Sonic data acquired while drilling can be used to estimate formation anisotropy that provide mechanical characterization of the drilled rock even before wireline sonic logging is performed. Estimated formation anisotropy can be indicators of the intrinsic anisotropy caused by microlayerings in shale together with stress- and fracture-induced anisotropies of the logged depth interval. Interpretation of formation anisotropy is critically dependent on the rock lithology and image logs that help to identify the presence of aligned fractures and thin beddings. Rock lithology helps to distinguish between microlayerings induced intrinsic shale and stress-induced anisotropy in sandstones and carbonates as a major source of observed anisotropy in the sonic data. Relative magnitudes of formation anisotropic constants are routinely used to classify anisotropy as a Transversely-Isotropic (TI) for a shale interval, or orthorhombic anisotropy associated with formations subject to triaxial stresses. While these tasks have been performed with open-hole logging using sonic data from wireline tools, it has not been possible to obtain a similar set of formation anisotropic constants using sonic data acquired during drilling. However, recently developed Logging-While-Drilling (LWD) sonic tools have the capability of providing estimates of formation anisotropic constants similar to those obtained with wireline sonic tools [12], [13], [14], [15], [16], [17], [18], [19], [20], [21], [22], [23], [24]. Processing and interpretation of data acquired by wireline sonic tools are relatively easier in the absence of any tool-based guided modes in the acquired data. In contrast, LWD sonic tools consist of a thick drilling collar that acts like a strong waveguide for elastic waves propagating along a liquid-filled borehole.

This article describes novel algorithms to invert measured collar-flexural and formation-flexural dispersions for a

subset of formation TI-constants that exhibits adequate dispersion sensitivity to these constants. The proposed algorithm accounts for the presence of a drill-collar in a LWD sonic tool. These techniques are based on model-based inversions of measured collar-flexural and formation-flexural dispersive modes generated by a dipole transmitter in a borehole surrounded by a fast or slow TI-formation.

II. METHODOLOGY

A. FORMATION ANISOTROPIC CONSTANTS FROM BOREHOLE GUIDED-MODE DISPERSIONS

An array of recorded waveforms at multiple receivers can be processed by a modified matrix pencil algorithm to isolate both non-dispersive and dispersive arrivals in the wavetrain [25]. This is a standard processing technique that helps to identify both the drill-collar and formation dominated dispersions from recorded waveforms generated by a dipole source in a LWD sonic tool. Both drill-collar and formation dispersions exhibit varying degrees of sensitivities to changes in the five TI-constants of the surrounding formation. Fractional changes in the borehole guided mode dispersions caused by changes in the formation TI-constants and mass density from a chosen Equivalent-Isotropic and Homogeneous (EIH) formation can be described by the following integral equation [8], [30]

$$\frac{\Delta V_k}{V_k^n} = \frac{\Delta\omega_k}{\omega_k^n} = \frac{\int_v dv \Delta C_{lmpq} u_{l,m}^n u_{p,q}^n dv}{2\left(\omega_k^n\right)^2 \int_v dv \rho_o u_q^n u_q^n dv} - \frac{\int_v dv \Delta\rho u_q^n u_q^n dv}{2\int_v dv \rho_o u_q^n u_q^n dv}, \quad (1)$$

where $\Delta V_k/V_k^n$ and $\Delta\omega_k/\omega_k^n$, respectively, represent fractional changes in the phase velocity and angular frequency at a given wavenumber k; the superscript n denotes the n-th mode of the liquid-filled borehole in the presence of a concentrically placed drill collar; ΔC_{lmpq} and $\Delta\rho$, respectively, denote differences in the elastic constants and mass density of the surrounding formation from those assumed in the reference EIH formation. In the sequel, we suppress the superscript n for brevity. The effective isotropic reference state can be described by the two Lamé constants λ and μ; and mass density ρ_o. The eigensolution for a chosen borehole mode n is denoted by the displacement u_q^n, and must be obtained in the presence of a concentrically placed thick drill collar in a liquid-filled borehole [28]. We have used Cartesian tensor notation for the elastic constants, a convention that a comma followed by an index q implies partial derivative with respect to x_q, and a summation convention for repeated indices. The Cartesian tensor indices l, m, p, and q take values 1, 2, and 3. Since the measured mass density is used in the chosen EIH reference state, there is no contribution from the second term in Eq. (1).

When specialized to a TI-anisotropy ($C_{11} = C_{22}$, $C_{44} = C_{55}$, $C_{12} = C_{11} - 2C_{66}$, $C_{13} = C_{23}$) with its symmetry axis parallel to the vertical X_3-axis, Eq. (1) can be reduced to the following form [6], [7], [8]

$$\frac{\Delta V_i}{V_i} = S_{11}^i \Delta C_{11} + S_{33}^i \Delta C_{33} + S_{55}^i \Delta C_{55} + S_{66}^i \Delta C_{66} + S_{13}^i \Delta C_{13}, \quad (2)$$

where

$$S_{tw}(k_i) = \frac{\int_v E_t E_w dv}{2\{\omega(k_i)\}^2 \int_v \rho_o u_q u_q dv}, \quad (3)$$

indices t and w denote the compressed Voigt's notation and take on values 1, 2, 3, ... 6, and the strain E_t is defined by

$$E_t \overset{def}{=} E_{pq} = \frac{1}{2}\left(u_{p,q} + u_{q,p}\right), \quad (4)$$

and u_p denotes the displacement associated with the eigensolution for either a collar or formation mode of a liquid-filled borehole in the presence of a drill collar. Note that the indices p and q in (4) denote the Cartesian tensor indices and take values 1, 2, and 3. These Cartesian tensor indices are replaced by Voigt's compressed notation following the convention: $11 \rightarrow 1, 22 \rightarrow 2, 33 \rightarrow 3, 23 \rightarrow 4, 13 \rightarrow 5$, *and* $12 \rightarrow 6$. The eigensolution u_p is calculated for a chosen equivalent-isotropic and homogeneous (EIH) formation defined by the measured formation bulk density, compressional and shear velocities. These plane wave velocities are then transformed into the two Lamé constants λ and μ, which are the isotropic elastic constants in the chosen reference state. The five unknowns ΔC_{11}, ΔC_{33}, ΔC_{55}, ΔC_{66}, and ΔC_{13} to be solved for in (2) are related to the five TI-constants at the logging depth as shown below

$$\begin{aligned} \Delta C_{11} &= C_{11} - (\lambda + 2\mu); \\ \Delta C_{33} &= C_{33} - (\lambda + 2\mu); \\ \Delta C_{55} &= C_{55} - \mu; \\ \Delta C_{66} &= C_{66} - \mu; \quad \text{and} \\ \Delta C_{13} &= C_{13} - \lambda. \end{aligned} \quad (5)$$

Since sensitivities of the measured guided-mode dispersion to the TI-constants C_{11} and C_{13} are relatively smaller than those for the other three TI-constants, it is necessary to construct difference equations at more than the minimum 5 wavenumbers (or frequencies). A matrix representation of these equations associated with the formation-flexural mode can be expressed as

$$\boldsymbol{A_f x} = \boldsymbol{b_f}, \quad (6)$$

where

$$\boldsymbol{x} = [\Delta C_{11}, \Delta C_{33}, \Delta C_{55}, \Delta C_{66}, \Delta C_{13}]^T = C_{tw} - x_{ref}, \quad (7)$$

$$\boldsymbol{b_f} = \left[\frac{\Delta V_1}{V_1}, \frac{\Delta V_2}{V_2}, \frac{\Delta V_3}{V_3}, \ldots \frac{\Delta V_i}{V_i}\right]^T, \quad (8)$$

$$\boldsymbol{A_f} = \begin{pmatrix} S_{11}^1 & \cdots & S_{13}^1 \\ \vdots & \ddots & \vdots \\ S_{11}^i & \cdots & S_{13}^i \end{pmatrix}, \quad (9)$$

C_{pq} represents the formation five TI-constants, x_{ref} denotes the isotropic reference TI-constants expressed in terms of the Lamé constants λ and μ, the superscript T denotes transpose of the row vector $\boldsymbol{x}$ containing 5 unknown TI-constants, and the input data $\boldsymbol{b_f}$ at wavenumbers $k_1, k_2, k_3, \ldots k_i\,(i > 5)$. The sensitivity matrix associated with the formation flexural dispersion is defined by $\boldsymbol{A_f}\,(i, 5)$, where the number of rows denoted by i must be greater than 5.

Likewise, another set of equations associated with the collar flexural dispersion takes the form

$$\boldsymbol{A_c x} = \boldsymbol{b_c}, \tag{10}$$

where the sensitivity matrix associated with the collar mode is defined by $\boldsymbol{A_c}\,(j, 5)$, and the index j denotes the number of input data $\boldsymbol{b_c}$ at wavenumbers $k_1, k_2, k_3, \ldots j\,(j > 5)$. Associated with the collar flexural dispersion.

B. JOINT INVERSION OF FORMATION-FLEXURAL AND COLLAR-FLEXURAL DISPERSIONS

Sonic logging-while-drilling is far more challenging than wireline logging where sonic slownesses (inverse of velocity) are measured after the drill collar has been taken out of the borehole. Sonic logging-while-drilling measurements are made in the presence of a drill collar (in the form of a thick steel pipe) that provides an additional path for the acoustic energy propagating from the transmitter to an array of hydrophone receivers. The goal of estimating formation compressional and shear slownesses becomes rather challenging because of a strong interference between the dominant collar and weak formation flexural modes in a fast formation as depicted in Fig. 2. Therefore, it is preferable to estimate Transversely-Isotropic (TI) formation anisotropic constants through joint inversion of the collar and formation dominated flexural dispersions, which helps to improve the inversion accuracy and also reduce uncertainty. For joint inversion, we introduce two inversion algorithms for comparison: (a) additive regularized Gauss-Newton inversion method with constraints; and (b) multiplicative regularized Gauss-Newton inversion method with constraints.

Generally, the sensitivity matrices $\boldsymbol{A_f}$ (and $\boldsymbol{A_c}$) are ill-conditioned because of widely varying sensitivities to different TI-constants. Under these circumstances, it is preferable to solve for the unknown vector $\boldsymbol{x}$ in a least-square sense by minimizing the norm $\left\|\boldsymbol{A_f x} - \boldsymbol{b_f}\right\|_2^2$. This cost function can be transformed to minimize $\left\|\boldsymbol{A_f}\tilde{\boldsymbol{x}} - \tilde{\boldsymbol{b}}_{\boldsymbol{f}}\right\|_2^2$, where

$$\tilde{\boldsymbol{x}} = \boldsymbol{C_{pq}}, \quad \textit{and}\ \tilde{\boldsymbol{b}}_{\boldsymbol{f}} = \boldsymbol{b} + \boldsymbol{A_f x_{ref}}. \tag{11}$$

Therefore, the modified cost function can be expressed as

$$f\,(\tilde{\boldsymbol{x}}) = \frac{\left(\boldsymbol{A_f}\tilde{\boldsymbol{x}} - \tilde{\boldsymbol{b}}_{\boldsymbol{f}}\right)^{\boldsymbol{T}}\left(\boldsymbol{A_f}\tilde{\boldsymbol{x}} - \tilde{\boldsymbol{b}}_{\boldsymbol{f}}\right)}{\boldsymbol{2}\left\|\tilde{\boldsymbol{b}}_{\boldsymbol{f}}\right\|_2^2} + \gamma^2\frac{\left(\tilde{\boldsymbol{x}} - \boldsymbol{x_{ref}}\right)^{\boldsymbol{T}}\left(\tilde{\boldsymbol{x}} - \boldsymbol{x_{ref}}\right)}{\boldsymbol{2}\left\|\boldsymbol{x_{ref}}\right\|_2^2}, \tag{12}$$

where the second term is an additive regularization and γ is the regularization coefficient [31].

Since the sensitivity matrix $\boldsymbol{A_f}$ is generally ill-conditioned, it is preferable to introduce additional constraints on the vector $\tilde{\boldsymbol{x}}$ to improve the accuracy of the inversion. To this end, we introduce a transformation pair for $\tilde{\boldsymbol{x}}$ and $\boldsymbol{m}$ as follows

$$\tilde{\boldsymbol{x}} = \tilde{\boldsymbol{x}}_{\boldsymbol{min}} + \frac{(\tilde{\boldsymbol{x}}_{\boldsymbol{max}} - \tilde{\boldsymbol{x}}_{\boldsymbol{min}})}{\boldsymbol{m^2 + 1}}\boldsymbol{m^2}, \tag{13}$$

$$\boldsymbol{m} = \left(\frac{\tilde{\boldsymbol{x}} - \tilde{\boldsymbol{x}}_{\boldsymbol{min}}}{\tilde{\boldsymbol{x}}_{\boldsymbol{max}} - \tilde{\boldsymbol{x}}}\right)^{\boldsymbol{1/2}}, \tag{14}$$

where $\tilde{\boldsymbol{x}}_{\boldsymbol{min}}$ and $\tilde{\boldsymbol{x}}_{\boldsymbol{max}}$ are the lower and upper bounds for $\boldsymbol{x}$, respectively. These transformations imply that

$$\begin{aligned} &\tilde{\boldsymbol{x}} \to \tilde{\boldsymbol{x}}_{\boldsymbol{min}}, \quad \textit{when}\ m \to 0, \ \text{and} \\ &\tilde{\boldsymbol{x}} \to \tilde{\boldsymbol{x}}_{\boldsymbol{max}}, \quad \textit{when}\ m \to \mp\infty. \end{aligned} \tag{15}$$

The cost function can now be written in terms of m as

$$f\,(\boldsymbol{m}) = \frac{\left(\boldsymbol{A_f}\tilde{\boldsymbol{x}} - \tilde{\boldsymbol{b}}_{\boldsymbol{f}}\right)^{\boldsymbol{T}}\left(\boldsymbol{A_f}\tilde{\boldsymbol{x}} - \tilde{\boldsymbol{b}}_{\boldsymbol{f}}\right)}{\boldsymbol{2}\left\|\tilde{\boldsymbol{b}}_{\boldsymbol{f}}\right\|_2^2} + \gamma^2\frac{\left(\boldsymbol{m} - \boldsymbol{m_{ref}}\right)^{\boldsymbol{T}}\left(\boldsymbol{m} - \boldsymbol{m_{ref}}\right)}{\boldsymbol{2}\left\|\boldsymbol{m_{ref}}\right\|_2^2}, \tag{16}$$

where $\boldsymbol{m_{ref}}$ can be calculated in terms of $\boldsymbol{x_{ref}}$ based on Eq. (14). Take derivative of cost function $f\,(\boldsymbol{m})$ with respect to $\boldsymbol{m}$

$$\frac{\partial f\,(\boldsymbol{m})}{\partial \boldsymbol{m}} = \frac{\left(\boldsymbol{A_f}\frac{d\tilde{\boldsymbol{x}}}{d\boldsymbol{m}}\right)^{\boldsymbol{T}}\left(\boldsymbol{A_f}\tilde{\boldsymbol{x}} - \tilde{\boldsymbol{b}}_{\boldsymbol{f}}\right)}{\left\|\tilde{\boldsymbol{b}}_{\boldsymbol{f}}\right\|_2^2} + \gamma^2\frac{\left(\boldsymbol{m} - \boldsymbol{m_{ref}}\right)}{\left\|\boldsymbol{m_{ref}}\right\|_2^2}, \tag{17}$$

which is a nonlinear equation in $\boldsymbol{m}$. Based on Gauss-Newton method, we can iteratively update the solution for m as follows

$$\left(\frac{\left(\boldsymbol{A_f}\frac{d\tilde{\boldsymbol{x}}}{d\boldsymbol{m}}\right)^{\boldsymbol{T}}\left(\boldsymbol{A_f}\frac{d\tilde{\boldsymbol{x}}}{d\boldsymbol{m}}\right)}{\left\|\tilde{\boldsymbol{b}}_{\boldsymbol{f}}\right\|_2^2} + \gamma^2\frac{\boldsymbol{I}}{\left\|\boldsymbol{m_{ref}}\right\|_2^2}\right)\Delta\boldsymbol{m} = -\left(\frac{\left(\boldsymbol{A_f}\frac{d\tilde{\boldsymbol{x}}}{d\boldsymbol{m}}\right)^{\boldsymbol{T}}\left(\boldsymbol{A_f}\tilde{\boldsymbol{x}} - \tilde{\boldsymbol{b}}_{\boldsymbol{f}}\right)}{\left\|\tilde{\boldsymbol{b}}_{\boldsymbol{f}}\right\|_2^2} + \gamma^2\frac{\left(\boldsymbol{m} - \boldsymbol{m_{ref}}\right)}{\left\|\boldsymbol{m_{ref}}\right\|_2^2}\right), \tag{18}$$

where $\Delta\boldsymbol{m} = \boldsymbol{m}_{n+1} - \boldsymbol{m}_n$, and $\boldsymbol{I}$ denotes a unit matrix. Once $\boldsymbol{m}$ is obtained through iterations, $\tilde{\boldsymbol{x}}$ can be calculated from Eq. (13). The aforementioned workflow can be also applied to invert either collar-flexural or formation-flexural dispersions for a subset of formation TI-anisotropic constants. This has been demonstrated using synthetic collar-flexural and

formation-flexural dispersions that are numerically exact and do not have any errors in them. This illustration serves as a validation of the proposed inversion algorithm with a proper choice of regularization coefficient γ as defined in Eq. (12).

Simultaneous inversion of the collar-flexural and formation flexural dispersions can be carried out using either (a) *Additive*, or (b) *Multiplicative* regularized Gauss-Newton inversion algorithm with prescribed constraints on the inverted anisotropic constants [31], [32], [33]. In addition, there are certain processing parameters, such as regularization coefficients must be optimized using synthetic data for a given class of formation anisotropy.

C. ADDITIVE REGULARIZED GAUSS-NEWTON ALGORITHM

A joint inversion of the collar-flexural and formation-flexural dispersions using an additive regularized Gauss-Newton algorithm is based on minimizing a cost function described by the following equation

$$f(\boldsymbol{m}) = \frac{\left(\boldsymbol{A_f}\tilde{\boldsymbol{x}} - \tilde{\boldsymbol{b}}_f\right)^T \boldsymbol{W}_f^T \boldsymbol{W}_f \left(\boldsymbol{A_f}\tilde{\boldsymbol{x}} - \tilde{\boldsymbol{b}}_f\right)}{2\left\|\tilde{\boldsymbol{b}}_f\right\|_2^2} + \frac{\left(\boldsymbol{A_c}\tilde{\boldsymbol{x}} - \tilde{\boldsymbol{b}}_c\right)^T \boldsymbol{W}_c^T \boldsymbol{W}_c \left(\boldsymbol{A_c}\tilde{\boldsymbol{x}} - \tilde{\boldsymbol{b}}_c\right)}{2\left\|\tilde{\boldsymbol{b}}_c\right\|_2^2} + \gamma^2 \frac{(\boldsymbol{m} - \boldsymbol{m_{ref}})^T (\boldsymbol{m} - \boldsymbol{m_{ref}})}{2\left\|\boldsymbol{m_{ref}}\right\|_2^2}, \tag{19}$$

where $\tilde{\boldsymbol{x}}$ and $\boldsymbol{m}$ are related to each other through transformation pairs (13) and (14). $\boldsymbol{A_f}$ and $\boldsymbol{A_c}$ are the sensitivity matrices of the formation and collar flexural modes. $\boldsymbol{W_f}$ and $\boldsymbol{W_c}$, respectively, are the weighting matrices associated with the formation and collar flexural modes. The third term is for regularization, and γ is the regularization coefficient. Note that the weighting matrices $\boldsymbol{W_f}$ and $\boldsymbol{W_c}$ should be chosen carefully to balance relative contributions between the flexural and collar modes to the formation anisotropic constants.

Take derivative of the cost function $f(\boldsymbol{m})$ with respect to $\boldsymbol{m}$

$$\frac{\partial f(\boldsymbol{m})}{\partial \boldsymbol{m}} = \frac{\left(\boldsymbol{A_f}\frac{d\tilde{\boldsymbol{x}}}{d\boldsymbol{m}}\right)^T \boldsymbol{W}_f^T \boldsymbol{W}_f \left(\boldsymbol{A_f}\tilde{\boldsymbol{x}} - \tilde{\boldsymbol{b}}_f\right)}{\left\|\tilde{\boldsymbol{b}}_f\right\|_2^2} + \frac{\left(\boldsymbol{A_c}\frac{d\tilde{\boldsymbol{x}}}{d\boldsymbol{m}}\right)^T \boldsymbol{W}_c^T \boldsymbol{W}_c \left(\boldsymbol{A_c}\tilde{\boldsymbol{x}} - \tilde{\boldsymbol{b}}_c\right)}{\left\|\tilde{\boldsymbol{b}}_c\right\|_2^2} + \gamma^2 \frac{(\boldsymbol{m} - \boldsymbol{m_{ref}})}{\left\|\boldsymbol{m_{ref}}\right\|_2^2}, \tag{20}$$

which is a nonlinear equation in $\boldsymbol{m}$. To solve for $\boldsymbol{m}$ iteratively using the Gauss-Newton method, we can update $\boldsymbol{m}$ as follows

$$\left(\frac{\left(\boldsymbol{A_f}\frac{d\tilde{\boldsymbol{x}}}{d\boldsymbol{m}}\right)^T \boldsymbol{W}_f^T \boldsymbol{W}_f \left(\boldsymbol{A_f}\frac{d\tilde{\boldsymbol{x}}}{d\boldsymbol{m}}\right)}{\left\|\tilde{\boldsymbol{b}}_f\right\|_2^2} + \frac{\left(\boldsymbol{A_c}\frac{d\tilde{\boldsymbol{x}}}{d\boldsymbol{m}}\right)^T \boldsymbol{W}_c^T \boldsymbol{W}_c \left(\boldsymbol{A_c}\frac{d\tilde{\boldsymbol{x}}}{d\boldsymbol{m}}\right)}{\left\|\tilde{\boldsymbol{b}}_c\right\|_2^2} + \gamma^2 \frac{\boldsymbol{I}}{\left\|\boldsymbol{m_{ref}}\right\|_2^2}\right) \Delta\boldsymbol{m} = -\left(\frac{\partial f(\boldsymbol{m})}{\partial \boldsymbol{m}}\right), \tag{21}$$

where $\Delta\boldsymbol{m} = \boldsymbol{m}_{n+1} - \boldsymbol{m}_n$. Once $\boldsymbol{m}$ is calculated from Eq. (21), the inverted $\tilde{\boldsymbol{x}}$ can be calculated from Eq. (13).

Note that following a conventional Gauss-Newton minimization approach, the second derivative of $\tilde{\boldsymbol{x}}$ with respect $\mathbf{m}$ is ignored in (18) and (21).

D. MULTIPLICATIVE REGULARIZED GAUSS-NEWTON ALGORITHM

The cost function for a multiplicative regularized Gauss-Newton algorithm can be written as

$$f(\boldsymbol{m}) = \frac{1}{2} f_1(\boldsymbol{m}) f_2(\boldsymbol{m}) f_3(\boldsymbol{m}), \tag{22}$$

where

$$f_1(\boldsymbol{m}) = \left(\boldsymbol{A_f}\tilde{\boldsymbol{x}} - \tilde{\boldsymbol{b}}_f\right)^T \boldsymbol{W}_f^T \boldsymbol{W}_f \left(\boldsymbol{A_f}\tilde{\boldsymbol{x}} - \tilde{\boldsymbol{b}}_f\right), \tag{23}$$

$$f_2(\boldsymbol{m}) = \left(\boldsymbol{A_c}\tilde{\boldsymbol{x}} - \tilde{\boldsymbol{b}}_c\right)^T \boldsymbol{W}_c^T \boldsymbol{W}_c \left(\boldsymbol{A_c}\tilde{\boldsymbol{x}} - \tilde{\boldsymbol{b}}_c\right), \tag{24}$$

$$f_3(\boldsymbol{m}) = \eta_n \left((\boldsymbol{m} - \boldsymbol{m_{ref}})^T (\boldsymbol{m} - \boldsymbol{m_{ref}}) + \delta^2\right), \tag{25}$$

$$\eta_n = (\boldsymbol{m}_n - \boldsymbol{m_{ref}})^T (\boldsymbol{m}_n - \boldsymbol{m_{ref}}) + \delta^2. \tag{26}$$

$f_1(\boldsymbol{m})$ and $f_2(\boldsymbol{m})$, respectively, are the cost functions associated with the formation-flexural and collar-flexural modes. $f_3(\boldsymbol{m})$ is the regularization term. $\boldsymbol{A_f}$ and $\boldsymbol{A_c}$ are the sensitivity matrices for the formation-flexural and collar-flexural dispersions, respectively. $\boldsymbol{W_f}$ and $\boldsymbol{W_c}$ are the corresponding weighting matrices. $\tilde{\boldsymbol{x}}$ and $\boldsymbol{m}$ are related to each other through the transformation pairs in Eqs. (13) and (14). δ is the regularization coefficient and η_n is the normalization coefficient at *n-th* iteration. We choose the weighting matrix $\boldsymbol{W_c}$ of the collar-flexural dispersion to be an identity matrix; and the weighting matrix $\boldsymbol{W_f}$ of the formation-flexural dispersion as $\|\boldsymbol{A_c}\|/\|\boldsymbol{A_f}\|$ times an identity matrix. This choice of weighting matrices provides balanced contributions from the collar and formation flexural dispersions to the measured input dispersion data.

The derivative of cost function $f(\boldsymbol{m})$ with respect to $\boldsymbol{m}$ can be expressed as

$$g(\boldsymbol{m}) = \frac{\partial f(\boldsymbol{m})}{\partial \boldsymbol{m}} = g_0 + f_1(\boldsymbol{m}) f_2(\boldsymbol{m}) \eta_n (\boldsymbol{m} - \boldsymbol{m_{ref}}), \tag{27}$$

where

$$g_0 = f_2(\boldsymbol{m}) \left(\boldsymbol{J}_f^T \boldsymbol{W}_f^T \boldsymbol{W}_f \left(\boldsymbol{A_f}\tilde{\boldsymbol{x}} - \tilde{\boldsymbol{b}}_f\right)\right) + f_1(\boldsymbol{m}) \left(\boldsymbol{J}_c^T \boldsymbol{W}_c^T \boldsymbol{W}_c \left(\boldsymbol{A_c}\tilde{\boldsymbol{x}} - \tilde{\boldsymbol{b}}_c\right)\right). \tag{28}$$

Therefore, the Hessian matrix H(m) takes the form

$$\begin{aligned}\boldsymbol{H}(\boldsymbol{m}) &= \frac{\partial g(\boldsymbol{m})}{\partial \boldsymbol{m}} \\ &\approx f_2(\boldsymbol{m})\boldsymbol{J}_f^T\boldsymbol{W}_f^T\boldsymbol{W}_f\boldsymbol{J}_f + f_1(\boldsymbol{m})\boldsymbol{J}_c^T\boldsymbol{W}_c^T\boldsymbol{W}_c\boldsymbol{J}_c \\ &\quad + f_1(\boldsymbol{m})f_2(\boldsymbol{m})\eta_n\boldsymbol{I} + 2\eta_n\left(\boldsymbol{m}-\boldsymbol{m}_{ref}\right)^T g_0\boldsymbol{I}, \quad (29)\end{aligned}$$

where $\boldsymbol{J}_f$ and $\boldsymbol{J}_c$ are the Jacobian matrices for the formation-flexural and collar-flexural dispersions, respectively. They are described as shown below

$$\boldsymbol{J}_f = \boldsymbol{A}_f\frac{d\tilde{\boldsymbol{x}}}{d\boldsymbol{m}}, \quad \boldsymbol{J}_c = \boldsymbol{A}_c\frac{d\tilde{\boldsymbol{x}}}{d\boldsymbol{m}}. \quad (30)$$

Based on a conventional Gauss-Newton iterative method, we can iteratively update $\boldsymbol{m}$ as follows

$$\boldsymbol{H}(\boldsymbol{m})\,\Delta\boldsymbol{m} = -g(\boldsymbol{m}), \quad (31)$$

where $\Delta\boldsymbol{m} = \boldsymbol{m}_{n+1} - \boldsymbol{m}_n$. Once $\boldsymbol{m}$ is calculated from Eq. (31), the inverted $\tilde{\boldsymbol{x}}$ can be calculated from Eq. (13).

E. SELECTION OF REGULARIZATION COEFFICIENTS

Generally, the collar-flexural and formation flexural dispersion sensitivity matrices are ill-conditioned and the measured dispersions from the field data also have some errors in them. Under these circumstances, constrained inversion algorithms with properly chosen regularization coefficients provide reliable estimates of a sub-set of TI-constants with adequate sensitivities to measured dispersions.

Since the regularization coefficient depends on the degree of ill-conditioning of the sensitivity matrices, it is suggested to optimally select the reference EIH formation parameters (by varying the reference shear velocity to within 1 to 5% of the measured shear velocity) that results in the lowest condition number of the sensitivity matrices $\mathbf{A_f}$ and $\mathbf{A_c}$. Next we start with an initial estimate of regularization coefficient as 0.25 that corresponds to an expected Gaussian noise of about 2 to 3% in the input (synthetic) dispersion. Smaller amounts of uncertainties in the input dispersion result in smaller values of regularization constant. For example, Gaussian noise level of about 0.5% results in an optimal regularization constant of 0.05. Continue to iteratively reduce the regularization coefficient to monitor the data misfit in terms of Relative Residual Errors between the reconstructed and input dispersions. Input dispersions are obtained from a root-finding mode-search routine for a concentrically placed drill collar in a liquid-filled borehole surrounded by a TI-formation with vertical axis of symmetry.

Another approach would be to vary the regularization coefficient on an empirical basis until the data misfit errors are reduced to an acceptable value.

Once a regularization coefficient has been determined for a given formation lithology, and expected amount of errors in the input (or measured) dispersions, this regularization coefficient can be fixed for other depths in the same lithology interval.

In summary, the procedure to estimate formation TI-anisotropy constants consists of the following steps:

1. Use the formation dipole shear velocity within 1 to 5% from the low-frequency asymptote of borehole flexural dispersions together with the measured formation compressional velocity and bulk density to generate a reference dipole flexural dispersion for an assumed EIH formation. Insofar as the formation bulk density as a function of depth is obtained from a neutron-density tool under in-situ conditions, there is no need to consider density perturbations from a chosen EIH reference state in (1).
2. Calculate wavenumber (or frequency) dependent sensitivities of the borehole flexural dispersions in the presence of a concentrically placed drill collar to the formation five TI-constants using a volumetric integral equation. The selection of shear velocity for the EIH formation can be optimized to obtain a low condition number of the flexural sensitivity matrix to facilitate improved accuracy of the inversion algorithm.
3. Invert differences between the measured and reference flexural dispersions over a chosen bandwidth for a subset of TI-constants that exhibit adequate sensitivities to measured dispersions.
4. Constrained inversion of flexural dispersions requires optimal selection of processing parameters based on synthetic data for a given class of formation anisotropy. A proper selection of frequency band for the inversion algorithm is an important input. The bandwidth selection is based on two factors: First, the usable bandwidths are strongly dependent on the LWD tool design, transmitter bandwidth, borehole mud, and formation lithology. Second, we select those bandwidths that exhibit larger sensitivities of measured dispersions to changes in the 5 TI-constants. As expected, bandwidths showing smaller sensitivities of input dispersions to changes in some of the TI-constants do cause larger variance in those inverted constants.
5. Terminate the iterative inversion process when the successive differences between the measured and predicted flexural dispersions using the inverted TI-constants become less than a chosen threshold.

III. ILLUSTRATIVE EXAMPLES WITH SYNTHETIC DATA

Synthetic collar and borehole guided modal dispersions can be generated by a root finding mode-search routine for a concentrically placed cylindrical layers in a liquid-filled borehole surrounded by an EIH formation [28], [29]. Elastic parameters for an EIH formation are defined by the measured formation bulk density, compressional headwave velocity, and shear velocity selected to be within 1 to 5% different than the formation shear velocity. These properties for an EIH formation ensure that actual anisotropic constants are perturbations from those assumed in the chosen EIH formation.

Fig. 1(a) shows schematic of a drill pipe concentrically placed in a liquid-filled borehole surrounded by an EIH formation. Note that the drill pipe inner and outer radii denoted by a and b, respectively; and its elastic properties can be

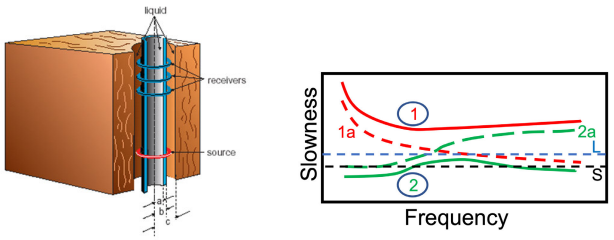

FIGURE 1. (a) Schematic diagram of a drill-collar concentrically places in a liquid-filled borehole surrounded by a formation. (b) Schematic diagram of the collar- flexural (upper red curve) and formation-flexural (lower green curve) dispersions in a FAST formation. Horizontal lines labeled L and S denote the borehole liquid compressional and formation shear slownesses, respectively.

selected to represent the entire LWD tool effects on the guided elastic wave propagation in a liquid-filled borehole of radius c.

A dipole source placed on the borehole axis generates both collar and formation dominated flexural modes. The composite structure of a drill-collar in a liquid-filled borehole can be analyzed in terms of two independent structures consisting of a drill-collar immersed in an infinite liquid, and a liquid-filled borehole surrounded by a formation. Curve 1a in Fig. 1(b) shows schematic of a collar-flexural dispersive mode supported by a drill-collar immersed in an infinite-liquid. Similarly, curve 2a depicts schematic of a formation-flexural dispersive mode associated with a liquid-filled borehole surrounded by a *fast formation* in the absence of any drill-collar. A crossing signature between these two dispersive modes implies a strong interference between the two modes in a composite structure of a drill-collar in a liquid-filled borehole. Curves labeled 1 and 2 in Fig. 1(b) denote the collar-flexural and formation-flexural dispersive modes, respectively, associated with the composite structure.

Guided flexural mode dispersions for (1) a steel pipe in an infinite liquid (in the absence of any formation); (2) a liquid-filled borehole surrounded by a formation (in the absence of a steel pipe); and (3) a steel pipe concentrically placed in a liquid-filled borehole surrounded by an isotropic formation have been calculated by a root-finding mode-search routine [9]. An overlay of collar-flexural dispersion for the case (1), and the formation-flexural dispersion for the case (2) associated with fast formations shows a crossing signature implying a strong interaction between these two modes for the case (3). These results for fast formations are summarized in Fig. 1(b). A strong interaction between the drill-collar and formation-flexural modes causes two coherent arrivals to be present over a wide frequency band in the processing window. It becomes necessary to use a model- based inversion algorithm to properly invert either of the two borehole guided dispersive modes for the formation anisotropic constants.

Inversion of formation-flexural dispersion for TI-constants in ***fast formations***

A dipole transmitter in a LWD sonic tool generates flexural waveforms that can be recorded by an array of receivers. These waveforms can be processed by a modified matrix pencil algorithm to identify both the formation-flexural and collar-flexural modes [25]. Both of these dispersive modes exhibit frequency-dependent sensitivities to a subset of TI-constants, C_{44} ($=C_{55}$), C_{66}, and C_{13} ($=C_{23}$).

We describe results from a *constrained inversion of formation-flexural dispersion for a sub-set of TI-constants of a fast formation*. Synthetic flexural dispersion has been obtained for an inner pipe radius $a = 3.5$ cm; outer pipe radius $b = 5.77$ cm concentrically placed in a borehole of radius $c = 10.16$ cm. The inner and outer drill-pipe radii may need to be optimized to make sure that the measured and predicted collar-flexural dispersions agree with each other in a chosen isotropic interval of the formation. These small perturbations in drill-pipe radii are required to account for the effects of tool-guts on the propagation of guided modes in the liquid-filled borehole. The inner and outer annuli of the drill-pipe is filled with water of mass density of 1 g/cc; and compressional velocity of 1500 m/s. Material parameters for the steel drill-pipe are defined by its mass density of 7.9 g/cc; compressional and shear velocities of 5800 m/s and 3100 m/s, respectively. Anisotropic constants of a fast TI-formation are summarized in Table 1; and its mass density is 2.35 g/cc.

TABLE 1. TI-constants of Bakken shale formation with X_3-symmetry axis.

C_{11} (GPa)	C_{13} (GPa)	C_{33} (GPa)	C_{55} (GPa)	C_{66} (GPa)
40.9	8.5	31.445	10.5	15.3

Since both the formation-flexural and collar-flexural dispersions have sensitivities to changes in the formation TI-constants, either one of them can be inverted to estimate a subset of TI-constants.

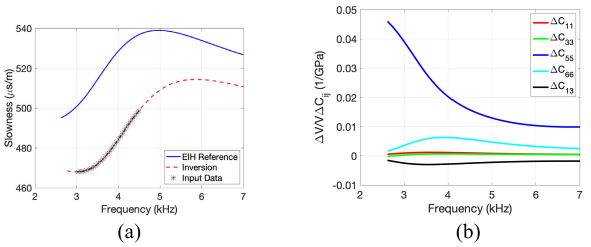

FIGURE 2. (a) The discrete * markers from about 3 to 4.5 kHz denote input data for *formation-flexural* dispersive mode. The EIH reference formation flexural dispersion (shown by the blue curve) is for an EIH formation with its elastic parameters close to the in-situ formation state. The dashed-red curve is the reconstructed formation-flexural dispersion using the inverted TI-constants. (b) *Formation-flexural* dispersion sensitivity to 1 GPa change in the 5 TI-constants of the surrounding Bakken shale formation. These sensitivity curves are calculated referred to a chosen EIH reference state of the formation.

The discrete * markers from about 3 to 4.5 kHz in Fig. 2(a) represent a bandlimited formation-flexural dispersive mode used as input to the inversion algorithm for estimating a subset of formation TI-constants. The blue curve in Fig. 2(a) shows a reference EIH formation-flexural dispersion. Referred to this EIH formation as a reference state, sensitivities of the formation flexural dispersions to the formation 5 TI-constants are determined from Eq. 3. Fig. 2(b) displays fractional changes in the flexural wave velocities caused by 1 GPa changes in the 5 TI-constants as a function of frequency. Observe that formation-flexural dispersion sensitivities to formation TI-constants are relatively larger at lower frequencies. Clearly, formation-flexural dispersion shows largest sensitivity to changes in the formation axial shear modulus C_{44}, followed by changes in the cross-sectional shear modulus C_{66} and an off-diagonal elastic constant C_{13}. Note that formation-flexural dispersion sensitivities to the compressional moduli C_{11} and C_{33} are rather small, and therefore, not good candidates for inversion. Nevertheless, the axial compressional modulus C_{33} can be reliably obtained from the refracted compressional headwave velocity.

The inverted constants obtained from the formation-flexural dispersion are $C_{66} = 15.6$ GPa; $C_{44} = 10.6$ GPa; $C_{13} = 8.88$ GPa; $C_{33} = 35.7$ GPa. Refracted compressional headwave velocity yields the compressional modulus $C_{33} = 36.5$ GPa. To validate the proposed inversion algorithm, the reconstructed formation-flexural dispersion using the inverted TI-constants is displayed by the dashed red curve in Fig. 2(b). Good agreement between the reconstructed and input (or measured) dispersions demonstrates the accuracy of the inversion algorithm with the numerically exact input dispersion.

Inversion of collar-flexural dispersion for TI-constants of ***fast formations***

Similar to the case of inverting the formation-flexural dispersion, calculate a reference collar-flexural dispersion for a selected EIH formation. Fig. 3(a) depicts the reference collar-flexural dispersion shown by the blue curve. Input to the inversion algorithm is a bandlimited collar-flexural dispersion from about 4 to 6 kHz shown by discrete * markers. Fig. 3(b) displays frequency-dependent collar-flexural dispersion sensitivities to the 5 TI-constants. Notice that collar-flexural sensitivities to formation TI-constants are larger at higher frequencies. Observe that collar-flexural dispersion sensitivities to the two compressional moduli C_{11} and C_{33} are somewhat different, and not negligibly small. As such, it is possible to invert for the 5 TI-constants using a constrained inversion algorithm as described earlier by Equations (10)-(18).

The inverted constants are $C_{66} = 15.7$ GPa; $C_{55} = 9.9$ GPa; $C_{13} = 8.52$ GPa; $C_{33} = 37.3$ GPa. Regularization coefficient $\gamma = 0.00035$. Inverted TI-constants are remarkably accurate when the input dispersion is obtained from the synthetic data shown by discrete * markers in Fig. 3(a), with no added noise. Good agreement between the inverted

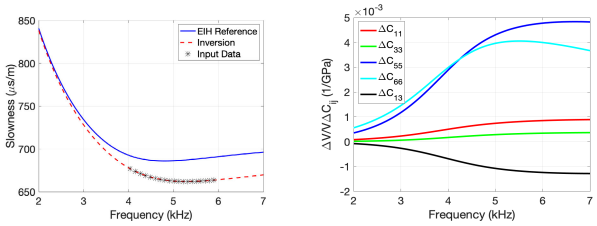

FIGURE 3. (a) The discrete * markers represent input dispersion data for *collar-flexural* dispersive mode. The EIH reference is from an equivalent isotropic homogeneous formation with its elastic properties close to the in-situ formation state. (b) *Collar-flexural* dispersion sensitivity to 1 GPa change in the 5 TI-constants of the surrounding Bakken shale. Notice large sensitivities at higher frequencies.

(dashed red curve) and input (discrete * markers) formation TI-constants as shown in Fig. 3(a), validates the accuracy and reliability of the proposed inversion algorithm. As noted earlier, the compressional modulus $C_{33} = 37.3$ GPa, is readily obtained from the compressional headwave velocity.

Joint inversion of formation-flexural and collar-flexural dispersions for TI-constants

Generally, both formation-flexural and collar-flexural dispersions obtained from field data have certain errors caused by the processing of dipole flexural waveforms obtained from a LWD sonic tool. Under these circumstances, inverting a formation-flexural or collar-flexural dispersions separately introduces larger uncertainties in the inverted constants. Therefore, it is desirable to implement a joint inversion of formation-flexural and collar-flexural dispersions for obtaining a subset of formation TI-constants. A joint inversion of two dispersions improves the reliability and accuracy of inverted TI-constants.

Below is a summary of joint inversion workflows for the *additive* and *multiplicative* algorithms:

1. Select an Equivalent-Isotropic and Homogeneous (EIH) formation close to the in-situ anisotropic formation properties.
2. Calculate both the collar-flexural and formation-flexural dispersion sensitivities to the 5 TI-constants referred to the selected EIH formation reference state.
3. *Additive Gauss-Newton inversion algorithm*: Optimally select the regularization coefficient γ by minimizing differences between the inverted and input TI-constants used to generate synthetic dispersions. Choice of the regularization coefficient γ depends on the condition numbers of dispersion sensitivity matrices and expected uncertainties in the input dispersion data.
4. *Multiplicative Gauss-Newton inversion algorithm:* Select relative weighting matrices $\boldsymbol{W_f}$ and $\boldsymbol{W_c}$ to balance contributions between the formation-flexural and collar-flexural dispersions to estimate formation anisotropic constants. In addition, the regularization coefficient δ and normalization coefficient η_n at *n-th* iteration need to be optimally selected to minimize

differences between the inverted and input TI-constants used to generate synthetic dispersions with added noise. Selection of the regularization coefficient depends on the dispersion sensitivity matrices and expected uncertainties in the input dispersion data.

5. Select different bandwidths for formation-flexural and collar-flexural dispersions that show largest sensitivities to some of the formation TI-constants.
6. Jointly invert differences between the measured and chosen EIH reference dispersions for a subset of TI-constants with larger sensitivities.
7. Accuracy of inverted TI-constants depends on the condition numbers of sensitivity matrices and accuracy of measured dispersions.

It is clear from Fig. 2(b), that the formation flexural mode has larger sensitivity at low frequency band (3∼4.5 kHz). In contrast, Fig. 3(b) shows that the collar flexural mode has larger sensitivity at high frequency band (4∼6 kHz).

With a proper choice of input dispersion data, inverted TI-constants from *additive* joint inversion of formation-flexural and collar-flexural dispersions are $C_{66} = 14.5$ GPa; $C_{55} = 10.7$ GPa; $C_{13} = 8.2$ GPa; $C_{33} = 37.3$ GPa; $C_{11} = 40.9$ GPa. Results are for a bandlimited input dispersion with 0.5% Gaussian noise added to the synthetic dispersion. Residual relative errors between the inverted and input formation-flexural and collar-flexural dispersions are 0.011 (with 28 measurements), and 0.033 (with 19 measurements), respectively. Regularization coefficient $\gamma = 0.05$.

Using the same choice of bandlimited input dispersion data as in the *additive* joint inversion algorithm and adding 1% Gaussian noise to the synthetic dispersion, inverted TI-constants from *multiplicative* joint inversion of formation-flexural and collar-flexural dispersions are $C_{66} = 15.5$ GPa; $C_{55} = 10.5$ GPa; $C_{13} = 10.1$ GPa; $C_{33} = 33.6$ GPa; $C_{11} = 41.1$ GPa. Both residual relative errors between the inverted and input formation-flexural and collar-flexural dispersions are 0.025 (with 28 measurements), and 0.056 (with 19 measurements), respectively. Regularization coefficient $\delta = 0.0195$.

The blue curve in Fig. 4(a) shows reference formation-flexural dispersion for an EIH formation with its elastic properties selected close to the in-situ formation state. Black * markers denote the input dispersion data from about 3 to 4.5 kHz, with 0.5% Gaussian noise added to the synthetic dispersion, and the black curve displays the reconstructed dispersion using inverted constants obtained from the *additive* joint inversion algorithm. Red * markers represent the input dispersion data with 1% Gaussian noise added to the synthetic dispersion, and the dashed-red curve depicts the reconstructed dispersion using the inverted constants obtained from the *multiplicative* joint inversion algorithm. Fig. 4(b) summarizes results from the inversion of collar-flexural dispersion with a proper selection of input bandlimited dispersion from about 4 to 6 kHz. The notation is same as in Fig. 4(a).

Good agreements between the reconstructed and input (measured) dispersions indicate the reliability of the proposed

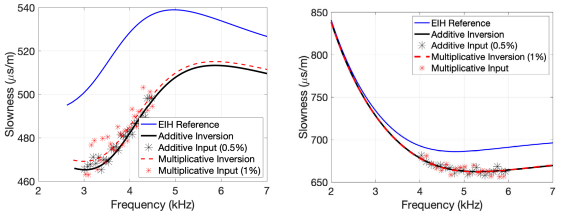

FIGURE 4. (a) The blue curve denotes reference formation-flexural dispersion for an EIH formation with its elastic properties selected close to the in-situ formation state. Black * markers show input dispersion data with 0.5% Gaussian noise added to the synthetic dispersion, and reconstructed dispersion using inverted constants shown by black curve obtained from the additive inversion algorithm. Red * markers denote corresponding inputs to the multiplicative inversion algorithm with 1% Gaussian noise added to the synthetic dispersion, and reconstructed dispersion shown by the dashed-red curve. (b) Results are from the inversion of collar-flexural dispersion. The notation is same as in Fig. 4(a).

additive and multiplicative inversion algorithms in the presence of added Gaussian noise to the input dispersion data.

*Inversion of collar-flexural dispersion for TI-constants of **slow formations***

Most of the flexural wave energy generated by a dipole transmitter is confined to the collar-flexural mode in slow formations. Generally, the collar-flexural mode exhibits significantly reduced sensitivity to formation TI-constants in *slow formations* than those in fast formations. In addition, it is rather difficult to measure formation-flexural dispersive mode in slow formations because of a rather weak coupling of the flexural waves generated by a dipole transmitter to this dispersive mode.

Therefore, it is imperative to develop an inversion algorithm for estimating a subset of slow formation TI-constants using only the collar-flexural mode dispersion with adequate sensitivity to at least some of the constants. Fig. 5(a) displays a typical collar flexural dispersion (red curve labeled 1) obtained from the LWD sonic tool data. The collar flexural dispersion (dashed red curve labeled 1a) is for a drill pipe in an infinite-liquid; and formation flexural dispersion (dashed-green curve labeled 2a) in the absence of any LWD tool in a liquid-filled borehole surrounded by slow formations.

As an illustrative example, we describe inversion results for a slow Austin chalk formation using synthetic collar-flexural dispersions without any noise, and with 0.5% Gaussian noise added to the synthetic dispersion. Table 2 contains the 5 TI-constants of the slow Austin chalk formation with mass density of 2.2 g/cc.

Fig. 5(b) depicts fractional changes in the collar-formation flexural wave velocity as a function of frequency caused by 1 GPa changes in the 5 TI-constants. The new inversion algorithm inverts the collar-formation flexural dispersion (red curve labeled 1) for a subset of TI-anisotropic constants (C_{55}, C_{66}, and C_{13}) by a proper selection of the bandwidth

TABLE 2. TI-constants of Austin chalk formation with X_3-symmetry axis.

C_{11} (GPa)	C_{13} (GPa)	C_{33}(GPa)	C_{55} (GPa)	C_{66} (GPa)
22.0	12.0	14.0	2.4	3.1

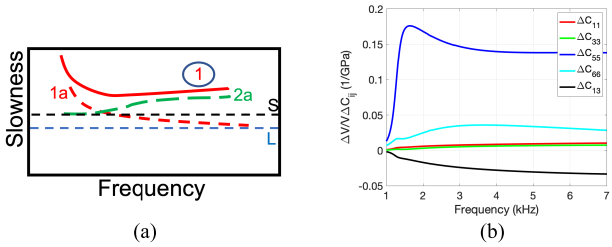

FIGURE 5. (a) Schematic diagram of the *collar* flexural dispersion shown by the red curve. The dashed red curve labeled 1a denotes the collar-flexural dispersive mode for a drill-collar immersed in an infinite liquid; and the dashed-green curve labeled 2a represents the formation-flexural dispersion in the absence of any tool in a borehole surrounded by a SLOW formation. Horizontal dashed lines labeled S and L denote the formation shear and borehole liquid compressional slownesses, respectively. (b) *Collar-formation* flexural dispersion sensitivity to 1 GPa change in the 5 TI-constants of the surrounding Austin chalk formation.

with relatively higher sensitivities to the three constants at higher frequencies, and adequate excitation levels. Notice that dispersion sensitivities to changes in the compressional moduli C_{11} and C_{33} are relatively smaller than those for the other three TI-constants. Therefore, it is not desirable to invert for these two compressional moduli in slow formations.

The discrete markers * in Fig. 6(a) denote synthetically generated collar-flexural dispersion from about 3 to 5 kHz. This dispersion data serves as input to the constrained inversion algorithm with optimally selected processing parameters. Inverted TI-constants for this example are summarized in Table 3. When the input dispersion data is numerically exact with no added noise, very good agreement between the inverted and input TI-constants validates the accuracy and reliability of the proposed algorithm.

TABLE 3. Inverted TI-constants of Austin chalk formation with X_3-symmetry axis using synthetic collar flexural dispersion without any Gaussian noise added to the input data.

C_{11} (GPa)	C_{13} (GPa)	C_{33}(GPa)	C_{55} (GPa)	C_{66} (GPa)
21.99	12.0	14.0	2.4	3.1

Fig. 6(b) displays results for the inverted TI-constants using synthetic collar-flexural dispersion with 0.5% Gaussian noise added to the input dispersion data. The discrete markers * in Fig. 6(b) represent the input dispersion data with added Gaussian noise. Constrained inversion processing parameters are optimized by minimizing relative residual errors between

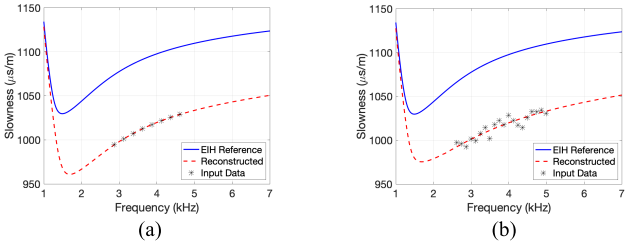

FIGURE 6. (a) Input *collar-flexural* dispersion data shown by discrete markers for *collar-flexural* dispersion without any noise added to the synthetic dispersion. The reference dispersion (blue curve) is for an EIH formation with its elastic properties selected close to the in-situ formation state. Dashed red curve displays reconstructed collar-flexural dispersion using inverted TI-constants. (b) Input collar-flexural flexural dispersion data shown by discrete * markers for *collar-flexural* mode with 0.5% Gaussian noise added to the synthetic dispersion. The reference dispersion (blue) is for an EIH formation with its elastic properties close to the in-situ formation state. Dashed red curve depicts reconstructed collar-flexural dispersion using inverted TI-constants.

TABLE 4. Inverted TI-constants of Austin chalk formation with X_3-symmetry axis using synthetic collar flexural dispersion with 0.5% Gaussian noise added to the input dispersion.

C_{13} (GPa)	C_{33} (GPa)	C_{55} (GPa)	C_{66} (GPa)
9.6 (25%)	14.2 (1.4%)	2.36 (1.6%)	3.20 (3%)

the reconstructed and synthetically generated input dispersions with added noise. Results for the inverted TI-constants from the constrained inversion algorithm are summarized in Table 4 (Regularization coefficient $\gamma = 0.02$). Differences between the inverted and input constants are shown in brackets. Accuracy of inverted TI-constants C_{44} and C_{66} are quite good. However, inverted C_{13} exhibits a large variance of up to 25%.

The dashed-red curve in Fig. 6(b) represents reconstructed collar-flexural dispersive mode using inverted TI-constants for this example. Good agreement has been obtained between the reconstructed and input dispersions with added noise. However, larger errors greater than 1% in the measured collar-flexural dispersion degrades reliable estimates of inverted TI-constants in slow formations.

IV. DISCUSSION

The proposed workflow yields a sub-set of TI-constants (C_{55}, C_{66}, and C_{13}) from a joint inversion of collar and formation flexural dispersions measured in fast TI-formations. The remaining two compressional moduli C_{11} and C_{33} exhibit relatively large errors, because of their rather small sensitivities to flexural dispersions. However, the axial compressional modulus C_{33} is, generally, obtained from the transit time of compressional headwaves generated by a monopole source. Estimates of these four TI-elastic constants as a function

of depth can then be used for geomechanical analysis of formations for maintaining wellbore stability during drilling, completion, and production of hydrocarbons.

Some challenges in a successful implementation of constrained inversion with an optimal choice of regularization coefficients include a proper selection of the reference EIH formation that yields flexural sensitivity matrix with low condition numbers; and optimal estimations of regularity coefficients based on expected noise in the measured dispersions. Higher values of regularity coefficients are needed to handle higher levels of noise in measured dispersions. Comparisons of the input and reconstructed dispersions (using inverted constants) have been done in terms of Relative Residual Errors (RRE). This amounts to show validity of the inverted results over the measurable bandwidth of input data. Optimal estimates of regularity coefficients are obtained by varying these coefficients from about 0.25 (in the presence of dispersion noise) to about 0.0005 (in the noise-free dispersion) until the data misfit or RRE is below a chosen threshold.

Generally, it is difficult to measure formation flexural dispersion in slow TI-formations. Most of the dipole transmitter energy is coupled to the propagating collar flexural mode. Consequently, the proposed workflow inverts the measured collar flexural dispersion for a subset of TI-constants (C_{33}, C_{55}, C_{66}, and C_{13}). Addition of Gaussian noise to the input (measured) dispersion degrades the accuracy of inverted constants. Higher accuracy in the inverted constants is obtained when the input dispersion is accurate and almost noise-free.

The feasibility of the proposed algorithm has been demonstrated using synthetic collar and formation flexural dispersion data, as well as with Gaussian noise added to these dispersions. Adding Gaussian noise to the input dispersion provides insight into the degradation of inverted quantities that might be reflected in the field data.

V. CONCLUSION

Formation anisotropic constants provide valuable information related to rock lithology, in-situ rock stresses, strengths, and natural or drilling-induced fractures. However, a proper interpretation of sonic-derived anisotropic constants must be carried out in conjunction with rock lithology determined from resistivity image logs and volumetric analysis of mineralogy [9], [10]. For instance, relative magnitudes of anisotropic constants are related to magnitudes of rock stresses only when the logged interval corresponds to clastic sandstones and carbonates. In contrast, certain relations among TI-constants estimated in a shale interval are indicators of microlayerings or thin laminations that are also observed in a resistivity image logs. Certain variations with depth in the rock stiffnesses or compliances from those in a TI-shale formation are indicators of existing natural fractures oriented either in the axial or cross-sectional planes of the borehole.

It has been demonstrated that the entire LWD tool can be modeled in terms of an equivalent drill pipe (or collar) with optimally selected inner and outer diameters, and appropriate elastic properties of pipe material. Under these circumstances, borehole elastic waves propagate as both drill collar and formation modes. It is then possible to identify these two traveling modes with their velocities exhibiting different frequency-dependent sensitivities to formation elastic properties. Constrained inversion algorithms have been developed to analyze the drill-collar or formation flexural modes separately or jointly, to estimate formation anisotropic constants. We highlight advantages of different choices in conjunction with frequency-dependent sensitivities to different formation TI-anisotropic constants. These inversion algorithms have been validated using synthetic data obtained for both fast and slow anisotropic formations in the presence of a generic LWD sonic tool. Hence, the proposed techniques provide novel workflows to invert collar-flexural and formation-flexural dispersive modes to estimate a sub-set of formation TI-constants.

ACKNOWLEDGMENT

The author Qingtao Sun was with Schlumberger-Doll Research.

REFERENCES

[1] B. K. Sinha and S. Zeroug, "Geophysical prospecting using sonics and ultrasonics," in *Wiley Encyclopedia of Electrical and Electronics Engineering*, vol. 8, J. G. Webster, Ed. New York, NY, USA: Wiley, 1999, pp. 340–365.

[2] V. Pistre and B. K. Sinha, "Applications of sonic waves in the estimation of petrophysical, geophysical and geomechanical properties of subsurface rocks," in *Proc. IEEE Ultrason. Symp.*, Beijing, China, Nov. 2008, pp. 78–85.

[3] G. Gao, A. Abubakar, and T. M. Habashy, "Borehole petrophysical imaging using induction and acoustic measurements," *Petrophysics*, vol. 54, no. 4, pp. 383–394, 2013.

[4] M. P. Ekstrom, C. A. Dahan, M. Y. Chen, P. M. Lloyd, and D. J. Rossi, "Formation imaging with microelectrical scanning arrays," *Log Anal.*, vol. 28, no. 3, p. 294, 1987.

[5] B. K. Sinha, A. N. Norris, and S. Chang, "Borehole flexural modes in anisotropic formations," *Geophysics*, vol. 59, no. 7, pp. 1037–1052, Jul. 1994.

[6] B. K. Sinha, A. Donald, J. Walsh, and T. Lei, "Anisotropic elastic constants from dipole flexural dispersions in unconventional shale-gas reservoirs," in *Proc. SEG Tech. Program Expanded Abstr.*, 2014, pp. 596–600, doi: 10.1190/segam2014-0193.1.

[7] B. K. Sinha and J. J. Walsh, "Orthorhombic elastic constants and mechanical properties for optimal completion of unconventional gas-shale reservoirs," in *Proc. SEG Tech. Program Expanded Abstr.*, Aug. 2015, pp. 684–688, doi: 10.1190/segam2015-5876362.1.

[8] B. K. Sinha, "Multi-frequency inversion of modal dispersions for estimating formation anisotropy constants," U.S. Patent 9 417 352 B2, Aug. 16, 2016.

[9] R. Prioul, A. Donald, R. Z. Koepsellm El Marzouki, and T. Bratton, "Forward modeling of fracture-induced sonic anisotropy using a combination of borehole image and sonic logs," *Geophysics*, vol. 72, pp. E135–E147, 2007, doi: 10.1190/1.2734546.

[10] R. Prioul and J. Jocker, "Fracture characterization at multiple scales using borehole images, sonic logs, and walkaround vertical seismic profile," *AAPG Bull. Special Session Fractures*, vol. 93, no. 11, pp. 1503–1516, Nov. 2009, doi: 10.1306/08250909019.

[11] C. V. Kimball and T. L. Marzetta, "Semblance processing of borehole acoustic array data," *Geophysics*, vol. 49, no. 3, pp. 274–281, 1984, doi: 10.1190/1.1441659.

[12] S. T. Chen, "Shear-wave logging with quadrupole sources," *Geophysics*, vol. 54, no. 5, pp. 590–594, May 1989.

[13] V. N. Rama Rao and J. K. Vandiver, "Acoustics of fluid-filled boreholes with pipe: Guided propagation and radiation," *J. Acoust. Soc. Amer.*, vol. 105, no. 6, pp. 3057–3068, Jun. 1999.

[14] C.-J. Hsu, J. A. Pabon, and B. K. Sinha, "Quadrupole shear wave logging while drilling," U.S. Patent 6 631 327 B2, Oct. 7, 2003.
[15] X. M. Tang, D. J. Patterson, T. Wang, J. V. Leggett, and V. Dubinsky, "Method and apparatus for LWD shear wave velocity measurement," U.S. Patent 6 985 086, Jan. 10, 2006.
[16] C.-J. Hsu, J. A. Pabon, B. K. Sinha, and S. Asvadurov, "Quadrupole acoustic shear wave logging while drilling," U.S. Patent 7 257 489 B2, Aug. 14, 2007.
[17] J. Alford, M. Blyth, E. Tollefsen, J. Crowe, J. Loreto, S. Mohamed, V. Pistre, and A. Rodriguez-Herrera, "Sonic logging while drilling–shear answers," *Oilfield Rev.*, vol. 24, no. 1, pp. 4–15, 2012.
[18] X. M. Tang, D. Patterson, V. Dubinsky, C. W. Harrison, and A. Bolshakov, "Logging-while-drilling shear and compressional measurements in varying environments," in *Proc. 44th Annu. Logging Symp. (SPWLA)*, Galveston, 2003, pp. 1–13.
[19] X. M. Tang, D. Vladimir, and J. P. Douglas, "Development of a low- frequency quadrupole shear-wave technology to improve quality of LWD shear velocity measurement," in *Proc. SPE Annu. Tech. Conf. Exhib.*, San Antonio, 2006, pp. 1–11.
[20] T. Kinoshita, T. Endo, H. Nakajima, H. Yamamoto, A. Dumont, and A. Hawthorn, "Next generation LWD sonic tool," in*Proc. 14th Formation Eval. Symp. Jpn.*, Japan, 2008, pp. 1–7.
[21] T. Kinoshita, A. Dumont, H. Hori, N. Sakiyama, J. Morley, and F. Garcia-Osuna, "LWD sonic tool design for high-quality logs," in *Proc. SEG Annu. Meeting*, pp. 513–517, 2010.
[22] J. Market and C. Bilby, "Introducing the first LWD crossed-dipole sonic imaging service," *Petrophys. J. Formation Eval. Reservoir Description (SPWLA)*, vol. 53, pp. 208–221, Jun. 2012.
[23] A. Oshima, D. Syresin, M. Blyth, and D. P. Schmitt, "Advanced dipole shear measurements with a new logging while drilling sonic tool," in *Proc. 59th Annu. Logging Symp. (SPWLA)*, London, U.K., Jun. 2018, pp. 1–8, Paper. SPWLA-2018-W.
[24] M. Blyth, "Revealing hidden information: High-resolution logging-while-drilling slowness measurements and imaging using advanced dual ultrasonic technology," *Petrophysics*, vol. 62, pp. 89–108, Feb. 2021.
[25] M. P. Ekstrom, "Dispersion estimation from borehole acoustic arrays using a modified matrix pencil algorithm," in *Proc. 29th Asilomar Conf. Signals, Syst., Comput.*, vol. 1, 1995, pp. 449–453.
[26] C.-J. Hsu and B. K. Sinha, "Mandrel effects on the dipole flexural mode in a borehole," *J. Acoust. Soc. Amer.*, vol. 104, no. 4, pp. 2025–2039, Oct. 1998.
[27] B. K. Sinha and S. Asvadurov, "Dispersion and radial depth of investigation of borehole modes," *Geophys. Prospecting*, vol. 52, pp. 271–286, Jun. 2004.
[28] B. K. Sinha, E. Simsek, and S. Asvadurov, "Influence of a pipe tool on borehole modes," *Geophysics*, vol. 74, no. 3, pp. E111–E123, May/Jun. 2009.
[29] E. Simsek and B. K. Sinha, "An efficient formulation for harmonic waves in multilayered cylindrical structures and its geophysical applications," in *Proc. 19th Int. Geophys. Congr. Exhib.*, Turkey, Ankara, 2010, pp. 1483–1486.
[30] B. K. Sinha, "Sensitivity and inversion of borehole flexural dispersions for formation parameters," *Geophys. J. Int.*, vol. 128, no. 1, pp. 84–96, Jan. 1997, doi: 10.1111/j.1365-246X.1997.tb04073.x.
[31] T. M. Habashy and A. Abubakar, "A general framework for constraint minimization for the inversion of electromagnetic measurements," *Prog. Electromagn. Res.*, vol. 46, pp. 265–312, 2004. doi: 10.2528/PIER03100702.
[32] F. O. Alpak, T. M. Habashy, A. Abubakar, C. Torres-Verdin, and K. Sepehrnoori, "A multiplicative regularized Gauss–Newton algorithm and its application to the joint inversion of induction logging and near-borehole pressure measurements," *Prog. Electromagn. Res. B*, vol. 29, pp. 105–138, 2011.
[33] A. Abubakar, M. Li, G. Pan, J. Liu, and T. M. Habashy, "Joint MT and CSEM data inversion using a multiplicative cost function approach," *Geophysics*, vol. 76, no. 3, pp. F203–F214, May 2011.

BIKASH K. SINHA (Life Fellow, IEEE) received the B.Tech. degree (Hons.) in mechanical engineering from the Indian Institute of Technology, Kharagpur, the M.A.Sc. degree in mechanical engineering from the University of Toronto, and the Ph.D. degree in applied mechanics from the Rensselaer Polytechnic Institute, Troy, NY, USA. He is currently a Retired Scientific Advisor and a Program Manager with Acoustics Research, Schlumberger-Doll Research, Cambridge, MA, USA. He held various assignments with Schlumberger spanning over four decades. He has made key contributions to the developments of dual-mode thickness-shear-based quartz pressure sensors for downhole measurements; and advancements of new inversion and interpretation techniques using borehole sonic data. He has authored or coauthored more than 220 technical articles. He received 67 U.S. patents in the areas of quartz pressure sensors, and borehole sonic and ultrasonic technologies in the oil and gas industry. He is a past member of the SEG, SPE, and SPWLA societies. He was a recipient of the 2015 IEEE Ultrasonics, Ferroelectrics, and Frequency Control Society Achievement Award and the 2012 IEEE International Frequency Control Symposium Cady Award for his contributions to the two domains of his expertise. He was a recipient of the Outstanding Paper Award for an article on dual-mode quartz pressure sensor published in the 1991 IEEE TRANSACTIONS ON ULTRASONICS, FERROELECTRICS, AND FREQUENCY CONTROL.

QINGTAO SUN received the B.S. and M.S. degrees in geo-detection and information technology from the China University of Petroleum, Qingdao, China, in 2009 and 2012, respectively, and the Ph.D. degree in electrical and computer engineering from Duke University, Durham, NC, USA, in 2017. His current research interests include numerical modeling techniques, electromagnetic and acoustic modeling for geophysical exploration, and inverse problems.